Korean J. Chem. Eng., 37(8), 1411-1418 (2020)
DOI: 10.1007/s11814-020-0606-2

pISSN: 0256-1115
eISSN: 1975-7220

Hybrid Pd_{38} nanocluster/$Ni(OH)_2$-graphene catalyst for enhanced HCOOH dehydrogenation: First principles approach

Dong Yun Shin*, Min-Su Kim*, Sukho Kang*, Jeong An Kwon*, Thillai Govindaraja*, Chang Won Yoon,***,†, and Dong-Hee Lim*,†**

*Department of Environmental Engineering, Chungbuk National University, Cheongju 28644, Korea
**Center for Hydrogen and Fuel Cell Research, Korea Institute of Science and Technology, Seoul 02792, Korea
***KHU-KIST Department of Converging Science and Technology, Kyung Hee University, Seoul 02447, Korea
(*Received 30 March 2020 • Revised 23 May 2020 • Accepted 4 June 2020*)

Abstract−Hydrogen energy is a potential next-generation energy source for fossil fuel replacement. The development of high-efficiency materials and catalysts for storage and transportation of hydrogen energy must be achieved to realize hydrogen economy. Recently, catalyst systems such as Pd nanoclusters (Pd NCs) supported on nickel hydroxide ($Ni(OH)_2$) have been reported to have advantages, including effective suppression of CO production and efficiency enhancement of HCOOH dehydrogenation. However, the reaction mechanism and multi-metallic interface system design of such systems have not been elucidated. Therefore, various $Ni(OH)_2$ surfaces supported on a graphene system were designed through density functional theory calculations, and the support material was combined with $Pd_{38}NC$ ($Pd_{38}NC/Ni(OH)_2$-G). Subsequently, the adsorption behavior of HCOOH dehydrogenation intermediates was analyzed. We found a new adsorption configuration in which HCOOH* (where * and a single underline indicates the adsorbed species and adsorbed atom, respectively) was adsorbed in a more stable manner (adsorption energy, E_{ads}= −1.22 eV) on the system than HCOOH* (E_{ads}=−1.10 eV) owing to the presence of $Ni(OH)_2$-G. This affected the next step in HCOOH dehydrogenation, i.e., formation of HCOO* species, and showed a positive effect on the HCOOH dehydrogenation. To fundamentally understand this phenomenon, electronic structure (d-band center and density of states) and stability (vacancy formation energy) analyses were performed.

Keywords: Formic Acid Dehydrogenation, Hydrogen Energy, Nickel Hydroxide, Density Functional Theory, Surface Stability

INTRODUCTION

The development of environmentally friendly energy sources is inevitable for solving the problem of global warming caused by the use of excessive fossil fuels. Among the various candidates, hydrogen (H_2) is a promising energy source owing to its cleanness, sustainability, and high energy density [1]. Numerous studies have been conducted using fuel cell technology to practically apply hydrogen energy to our social infrastructure.

Formic acid (HCOOH) has been verified as an excellent liquid hydrogen storage material owing to its low toxicity and high hydrogen content (4.4 wt%) [2,3]. Hydrogen can be controllably released through HCOOH dehydrogenation (ΔG=−32.8 kJ mol^{-1}) at room temperature in the presence of a suitable catalyst [4,5]. Among various metal catalysts for HCOOH dehydrogenation, palladium (Pd) has been reported as the best catalyst, showing excellent hydrogen production [6,7]. However, HCOOH dehydrogenation on Pd catalysts is capable of generating CO, which can lower the catalytic efficiency. This phenomenon has been controlled by designing new Pd based catalysts (e.g., alloys, core-shall nanoparticles, and nanoclusters (NCs) supported on graphene), and even the catalysts were shown to be more efficient and economical than conventional Pd surfaces [8,9].

Recently, multi-metallic nanocatalysts have attracted considerable attention as catalysts for hydrogen production because of their significant synergistic effect from their multi-component interfacial active sites [10-15]. Precisely, the introduction of non-noble metal hydroxides to form multi-metallic nanostructures cannot only minimize the use of noble metals but also enhance the catalytic performance [10-13]. Previous studies reported that hybrid $Pt/FeNi(OH)_x$ nanoparticles exhibited high performance for CO oxidation [10], $Pt/M(OH)_2$ (M=Ni, Co) nanoparticles were significantly able to enhance the activity of the hydrogen evolution reaction [12]. Additionally, subnanometric hybrid $Pd\text{-}M(OH)_2$ (M=Ni, Co) clusters encapsulated within purely siliceous zeolites showed superior thermal stability at 600-700 °C and complete HCOOH dehydrogenation without using any additives at 60 °C [15]. In addition, graphene supports, which can modify the electronic properties of a catalyst in positive ways, have been widely used to improve the activity and efficiency of metal catalysts [16-22]. For example, graphene-supported Cu nanoparticles showed the enhanced efficiency of conversion of CO_2 into hydrocarbon fuels, which was attributed to the electronic properties of graphene [23]. Shin et al. [24] reported that nitrogen-doped graphene-supports could improve the efficiency of formate ($HCOO^-$) and bicarbonate (HCO_3^-) reversible reactions by modifying the electronic and geometrical properties of Pd nanopar-

†To whom correspondence should be addressed.
E-mail: limkr@cbnu.ac.kr, cwyoon@kist.re.kr
Copyright by The Korean Institute of Chemical Engineers.

ticles. The graphene supports also had a positive influence on the formation of nickel hydroxide ($Ni(OH)_2$) nanoplates with excellent electrochemical properties and stability [25].

Innovative catalysts combining multi-metallic nanocatalysts and graphene support, with the aforementioned advantages, have tremendous potential for improving the efficiency of HCOOH dehydrogenation. However, analyzing the catalyst involves many difficulties due to the lack of related research and the complex structural properties of various elements. Therefore, it is necessary to clearly understand the structural properties of the new catalysts and the adsorption behavior of HCOOH dehydrogenation intermediates. In this study, we designed a large-scale metallic NC supported on a graphene system ($Pd_{38}NC/Ni(OH)_2$-G), which can be compared with experiments, and we investigated the adsorption behavior of intermediates for enhancing the efficiency of HCOOH dehydrogenation, using density functional theory (DFT) calculations. This can provide important insight into future study on hydrogen storage and production related to HCOOH dehydrogenation as well as the development of complex structured multi-metallic catalysts applicable to various energy domains.

COMPUTATIONAL METHODOLOGY

All spin-polarized DFT+*U* calculations were carried out using the Vienna ab initio Simulation Package (VASP) [26,27] with the projector augmented wave (PAW) [27,28] method. The Perdew-Burke-Ernzerhof (PBE) functional [29] with the generalized gradient approximation (GGA) was used to describe the electron exchange correlation functions. A kinetic energy cutoff for the plane-wave basis sets was set at 300 eV in all calculations considering the large size of the system. Brillouin zone integration was performed on a 16×16×16 (bulk) and 4×2×1 (surface system) Monkhorst-Pack grid [30], respectively. The first-order Methfessel-Paxton smearing [31] with a value of 0.1 eV was applied. The Hubbard-*U* term of 3.8 eV was employed to correct the error of overdelocalization of electrons, of transition metal oxides [32]. The DFT-D2 method was selected to accurately simulate the van der Waals (vdW) forces [33].

The $Pd_{38}NC$-$Ni(OH)_2(100)$-graphene ($Pd_{38}NC/Ni(OH)_2$-G) system was designed based on a 13.06×25.76×25.00 Å orthorhombic supercell with periodic boundary conditions. The $Pd_{38}NC/Ni(OH)_2$-G system consisted of 277 atoms and the $Pd_{38}NC$ (38 Pd atoms) was adsorbed on a single-layer of $Ni(OH)_2(100)$ (23 $Ni(OH)_2$ bulks) supported on graphene (124 carbon atoms). The octahedral $Pd_{38}NC$ was selected based on the magic numbers, considering the surface size of the designed $Ni(OH)_2$-G. Although $Pd_{38}NC$ may be included in an NC consisting of magic numbers (7, 13, 55, etc.) [34], it provides flat adsorption surfaces that can effectively prevent overestimation of adsorption behavior and energy. Furthermore, $Pd_{38}NC$ has a comparable stability to an NC consisting of atoms with magic numbers in terms of binding energy per atom (Pd_{13}, Pd_{38} and Pd_{55}=220, 274 and 288 kJ/mol, respectively) [35]. This consideration is supported by previous studies that have accurately analyzed the adsorption behavior by utilizing NCs providing flat adsorption sites [24,36].

The single-layer $Ni(OH)_2(100)$ supported on graphene was designed to not only minimize the lattice constant mismatch between $Ni(OH)_2$ and graphene but also to provide an appropriate adsorption site for adsorbing $Pd_{38}NC$s. Tensile and compressive strain effects were observed between $Ni(OH)_2$ and graphene owing to the lattice mismatch.

All atoms of the $Pd_{38}NC/Ni(OH)_2$-G system were fully relaxed and optimized until the convergence criterion for electronic self-consistent iteration was less than 10^{-4} eV. However, when calculating the adsorption models, atoms were partially fixed except for interfacial sites between $Pd_{38}NC$s and $Ni(OH)_2$-G for the interaction of adsorbates, considering computing resources and time. The gas-phase molecules were optimized using Brillouin zone integration with only the Γ-point under the same conditions as those used of the surface system.

The adsorption energy (E_{ads}) and vacancy formation energy (E_{vac}) are defined as Eq. (1) and (2), respectively.

$$E_{ads}=E_{substrate+adsorbate}-E_{substrate}-E_{adsorbate} \quad (1)$$

$$E_{vac}=E_{defective\ substrate}+E_{atom}-E_{pristine\ substrate} \quad (2)$$

In Eq. (1), $E_{substrate+adsorbate}$, $E_{substrate}$, and $E_{adsorbate}$ are the total DFT energies of a substrate and adsorbate ($Pd_{38}NC/Ni(OH)_2$-G adsorbed HCOOH), substrate ($Pd_{38}NC/Ni(OH)_2$-G), and gas-phase adsorbate (HCOOH), respectively. A negative adsorption energy value indicates that the adsorption is stable. In Eq. (2), $E_{defective\ substrate}$, E_{atom}, and $E_{pristine\ substrate}$ are the DFT energies of defective $Pd_{38}NC/Ni(OH)_2$-G, Pd atom divided by the number of atoms of bulk Pd, and pristine $Pd_{38}NC/Ni(OH)_2$-G, respectively. A positive vacancy formation energy indicates that the surface system is stable.

RESULTS AND DISCUSSION

In this section, we discuss the novel design of the $Pd_{38}NC/Ni(OH)_2$-G systems and analyze the adsorption behavior of the intermediate species of HCOOH dehydrogenation on $Pd_{38}NC/Ni(OH)_2$-G and $Pd_{38}NC$ systems, proposing a possible dehydrogenation pathway for HCOOH. In addition, we explain the results of electronic structure (density of states) and durability (Pd vacancy formation energy) analyses to understand the fundamental reason for the positive effect of $Ni(OH)_2$-G on HCOOH dehydrogenation.

1. Design of $Pd_{38}NC/Ni(OH)_2$-graphene System

To design $Pd_{38}NC/Ni(OH)_2$-graphene, we first optimized the bulk structures of $Ni(OH)_2$ and graphene. The optimized lattice constants of bulk $Ni(OH)_2$ were 3.16 Å (a=b) and 4.45 Å (c), respectively (Fig. 1(a)), which were in agreement with the experimental values (3.12 Å and 4.66 Å, respectively) [37]. In the case of graphene, the C-C distance was calculated to be 2.47 Å (Fig. 1(c)), which agreed with the experimental value (2.46 Å) [38].

Graphene-supported $Ni(OH)_2$ has been reported to show excellent cycling stability and electrochemical characteristics [25,39]. Because $Ni(OH)_2$ has various surfaces, it is necessary to select a suitable surface to simulate it by using DFT calculations. As the most suitable surfaces for combining with graphene, we selected four $Ni(OH)_2$ surface models such as (001), (100), (101), and (110) surfaces (Fig. S1 in Supporting Information (SI)) based on the previous X-ray diffraction (XRD) analysis [40] demonstrating the highest

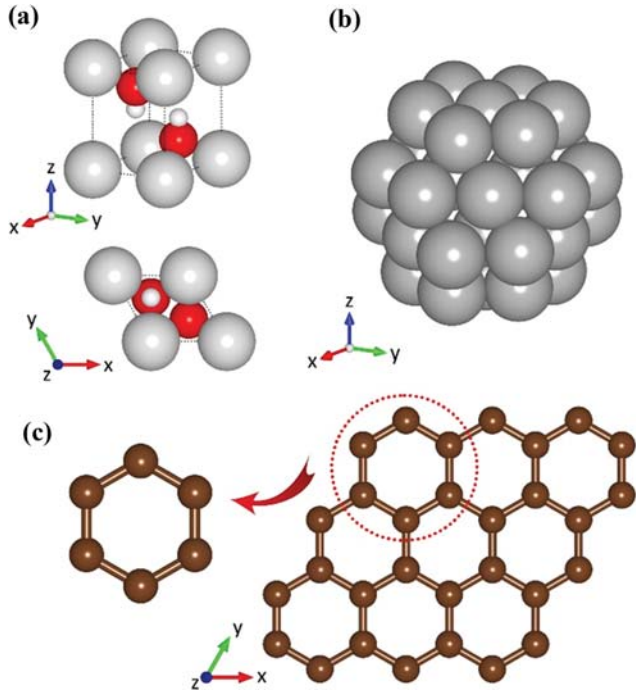

Fig. 1. Optimized structures of (a) bulk $Ni(OH)_2$ (side and top views), (b) clean $Pd_{38}NC$ (side view), and (c) bulk and extended graphene (top view). Light grey, dark grey, red, white, and brown spheres represent Ni, Pd, O, H, and C, respectively.

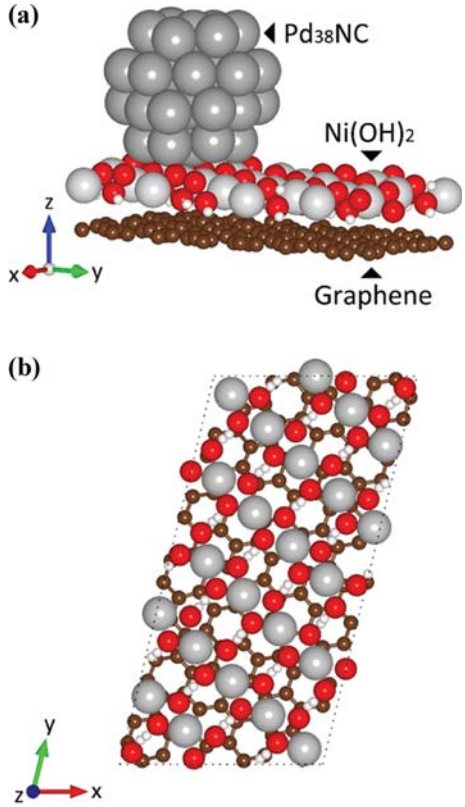

Fig. 2. Optimized structures of (a) the $Pd_{38}NC/Ni(OH)_2$(100)-graphene (side view) system, and (b) the $Ni(OH)_2$(100)-graphene (top view). Light grey, dark grey, red, white, and brown spheres represent Ni, Pd, O, H, and C, respectively.

XRD peak intensities of the selected facets. When designing $Ni(OH)_2$-G, the strain effect was applied to the $Ni(OH)_2$ surfaces which were placed on graphene because of the complex design properties such as the number of atoms, the size of the surface area, and the adsorption angle between the surfaces. A total of four candidates were designed for each surface, and the selection criteria of surfaces that could represent each surface were set to the minimum lattice constant mismatch and the number of atoms constituting the system. The designed $Ni(OH)_2$(001), (100), (101), and (110)-G consisted of 214 atoms with 0.63% compressive strain, 239 atoms with 0.61-0.70% tensile strain, 213 atoms with 0.14% compressive strain, and 215 atoms with 0.53-0.73% tensile strain, respectively. Detailed structures of other candidates are shown in the SI section 1.

The $Pd_{38}NC/Ni(OH)_2$(100)-G system was selected as the surface model for this HCOOH dehydrogenation study (Fig. 2(a)). This was because other systems such as $Pd_{38}NC/Ni(OH)_2$(001, 101 and 110) showed the dissociation of hydrogen atoms from the $Ni(OH)_2$-G surface when $Pd_{38}NC$ was adsorbed on the support, collapsing the Pd-$Ni(OH)_2$ system due to the mismatch of the system components. Although the $Ni(OH)_2$(001) surface was reported to be the most stable surface [40], Qi et al. [41] reported that the (100) surface was also efficiently formed on graphene. In addition, the selected $Ni(OH)_2$(100) surface provided sufficient surface area for adsorbing $Pd_{38}NC$.

2. Adsorption Behavior of HCOOH Dehydrogenation Intermediates

The adsorption configuration of HCOOH and the intermediate species in the HCOOH dehydrogenation reaction pathway are important factors for determining the dehydrogenation efficiency. Previous studies have reported that HCOOH dehydrogenation proceeds through two reaction pathways, HCOO (two O atoms are adsorbed) and COOH (O and H atoms are adsorbed) pathways, of which the HCOO pathway has shown a higher dehydrogenation efficiency than the COOH pathway [42]. This is because HCOOH dehydrogenation through the COOH pathway offers the possibility that CO can be produced, which can lower the efficiency of the catalysts [42]. Therefore, many researchers are developing catalysts suitable for HCOOH dehydrogenation through the HCOO pathway.

We focused on the analysis of HCOOH adsorption configurations, the most important adsorbate of HCOOH dehydrogenation, which determines further reaction pathways of the HCOOH dehydrogenation. Fig. 3 shows various adsorption models of HCOOH and their adsorption energy values. The notable points are that HCOOH was more strongly adsorbed on $Pd_{38}NC/Ni(OH)_2$-G than on $Pd_{38}NC$. Additionally, the $\underline{H}COO\underline{H}_b$* (where * and a sign underline indicate the adsorbed species and adsorbed atom on the surface, respectively) in which two H atoms were adsorbed on $Pd_{38}NC/Ni(OH)_2$-G system was the most stable (E_{ads}=−1.22 eV, Fig. 3(e)).

Another important finding is that in the $Pd_{38}NC/Ni(OH)_2$-G system, the adsorbates ($\underline{H}COO\underline{H}_b$*, $\underline{H}C\underline{O}O_b$*, $C\underline{O}O\underline{H}$*, and H*) that mainly interacted with the surface through their H atoms were strongly adsorbed, but those interacting through their O atoms

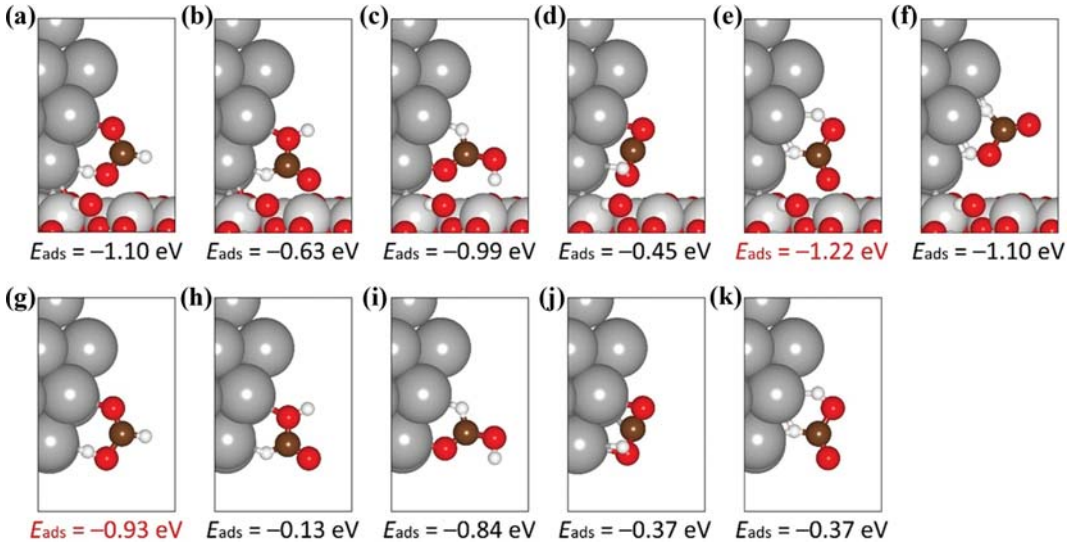

Fig. 3. Comparison of adsorption energy values of HCOOH on $Pd_{38}NC/Ni(OH)_2(100)$-G system (a)-(f) and clean $Pd_{38}NC$ (g)-(k).

Table 1. Adsorption energy (E_{ads}) of intermediates of HCOOH dehydrogenation. $HC\underline{O}O\underline{H}_a$, $\underline{H}COO\underline{H}_b$, $HC\underline{O}\underline{O}_a$, and $\underline{H}C\underline{O}O_b$ are adsorption configurations in which one H atom, two H atoms, two O atoms, and one O atom are adsorbed on a surface

Adsorbates	E_{ads} (eV)	
	$Pd_{38}NC/Ni(OH)_2$-G	$Pd_{38}NC$
$HC\underline{O}O\underline{H}_a$*	−1.10	−0.93
$\underline{H}COO\underline{H}_b$*	−1.22	−0.37
$HC\underline{O}\underline{O}_a$*	−3.52	−3.73
$\underline{H}C\underline{O}O_b$*	−4.57	−3.10
$C\underline{O}O\underline{H}$*	−1.36	−0.74
H*	−1.34	−0.62

were weakly adsorbed (Table 1). These adsorption properties can facilitate their stable formation. However, in the case of the H* adsorption, a stronger adsorption of H may negatively affect the desorption of H to produce H_2(g) as the final product.

3. Comparison of HCOOH Dehydrogenation in the HCOO Pathway

The conventional HCOO pathway of HCOOH dehydrogenation has been reported as $HC\underline{O}O\underline{H}_a$*→$HC\underline{O}\underline{O}_a$*+H*→$\underline{H}C\underline{O}O_b$*→$CO_2$*+$H_2$* (1→3→4→5 in Fig. 4). In this conventional HCOO pathway, $HC\underline{O}\underline{O}_a$* rotates to form $\underline{H}C\underline{O}O_b$*, which is advantageous for proceeding to the CO_2*+H_2* step, thus improving the efficiency of H_2(g) production by decreasing the activation energy. Recently, Wang et al. [43] reported that the HCOOH dehydrogenation steps for H_2(g) production can be significantly influenced by the initial adsorption configuration of HCOOH. They proposed a direct HCOO pathway (2→4→5 in Fig. 4) that did not involve the highest energy barrier step of the HCOO* rotation, especially when a specific promoter was present. The direct HCOO pathway could significantly enhance the efficiency of HCOOH dehydrogenation by skipping the $HC\underline{O}\underline{O}_a$*+H* step, thereby shortening the

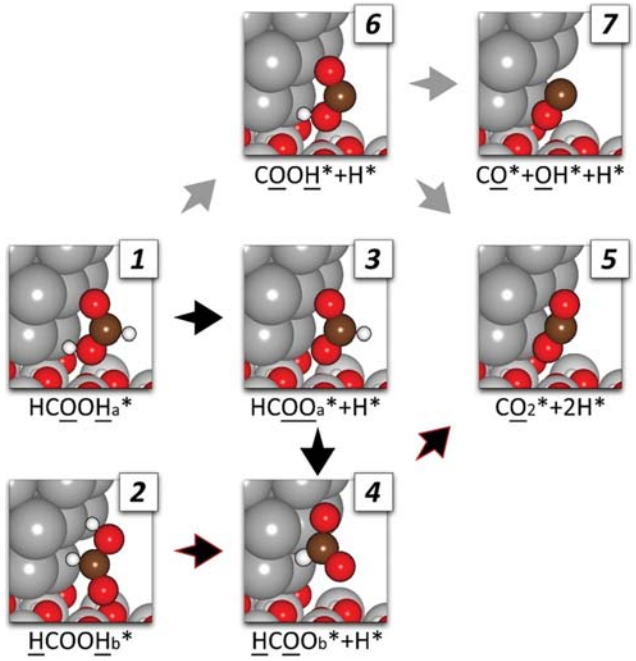

Fig. 4. HCOOH dehydrogenation through the conventional HCOO (1→3→4→5), direct HCOO (2→4→5), and COOH (1→6→5 or 7) pathways on the $Pd_{38}NC/Ni(OH)_2$-G system. A single underline represents the adsorbed atom on the surface.

reaction steps directly, such as $\underline{H}COO\underline{H}_b$*→$\underline{H}C\underline{O}O_b$*+H*→$CO_2$*+$H_2$* [43].

Fig. 4 indicates that the HCOOH dehydrogenation can occur through the HCOO or COOH pathway. According to the adsorption energy values of HCOO and COOH in both catalytic systems, the adsorption strength of COOH was significantly lower than that of HCOO, indicating that the HCOO pathway would be more preferred to the COOH pathway (1→6→5 or 7 in Fig. 4). Examining the adsorbed configurations of HCOO* in both catalytic

Table 2. Comparison of bond lengths of adsorbed species

Adsorbates		C-H (Å)	O-H (Å)	C=O (Å)	C-O (Å)
$HC\underline{O}O\underline{H}_a$(g)		1.0797	0.9917	1.2044	1.3599
$\underline{H}COO\underline{H}_b$(g)		1.1434	0.9647	1.2284	1.4276
$Pd_{38}NC/Ni(OH)_2$-G	$HC\underline{O}O\underline{H}_a$*	1.0896	1.0068	1.2347	1.2297
	$\underline{H}COO\underline{H}_b$*	1.1581	1.0122	1.2158	1.3567
	$HC\underline{OO}_a$*	1.1032	-	1.2535	1.2024
	$\underline{H}C\underline{O}O_b$*	1.1194	-	1.1973	1.3685
	$C\underline{O}O\underline{H}$*	-	1.0154	1.2276	1.2238
$Pd_{38}NC$	$HC\underline{O}O\underline{H}_a$*	1.1048	1.0265	1.2606	1.3567
	$\underline{H}COO\underline{H}_b$*	1.1631	1.0112	1.2225	1.3610
	$HC\underline{OO}_a$*	1.0870	-	1.2413	1.2853
	$\underline{H}C\underline{O}O_b$*	1.1258	-	1.1956	1.3694
	$C\underline{O}O\underline{H}$*	-	1.0203	1.2267	1.2203

systems, the $Pd_{38}NC$ and $Pd_{38}NC/Ni(OH)_2$-G systems follow the conventional HCOO and direct HCOO pathways, respectively. In addition, the $HC\underline{OO}_a$*+H*→$\underline{H}C\underline{O}O_b$*+H* step of $Pd_{38}NC$ was endothermic because the adsorption energy values of $HC\underline{OO}_a$* and $\underline{H}C\underline{O}O_b$* were −3.73 and −3.10 eV, respectively. However, in the case of $Pd_{38}NC/Ni(OH)_2$-G, the $\underline{H}C\underline{O}O_b$* adsorption strength was significantly stronger than that of $HC\underline{OO}_a$*, indicating that $\underline{H}C\underline{O}O_b$* can be directly formed without forming the $HC\underline{OO}_a$* species, which implies that HCOOH dehydrogenation in the $Pd_{38}NC/Ni(OH)_2$-G system may follow the direct HCOO pathway. This finding suggests that the $Pd_{38}NC/Ni(OH)_2$-G system may improve the efficiency of HCOOH dehydrogenation by shortening the reaction step of the HCOO pathway without additional additives.

Despite the evidence of the adsorption behavior of HCOOH and intermediate species in both catalytic systems, a limitation may lie in the comparison of the HCOOH dehydrogenation efficiency. This may be due to the absence of activation energy calculations, which might be impractical for DFT calculations with such a large system of $Pd_{38}NC/Ni(OH)_2$-G (consisting of 277 atoms). However, the large adsorption energy difference in both catalytic systems may rationally support the current conclusion of this study.

Additionally, when the adsorbate is adsorbed on the surface, the change in the bond length between atoms having the adsorbate can be an indicator for predicting the next step [44]. In this study, the O-H bond of $HC\underline{O}O\underline{H}_a$* has been activated to form $HC\underline{OO}_a$*+H* on $Pd_{38}NC$, having a bond length higher (3.51%) than that of $Pd_{38}NC/Ni(OH)_2$-G (1.52%) system, whereas the O-H bond length of $\underline{H}COO\underline{H}_b$* has been activated to form $\underline{H}C\underline{O}O_b$*+H* on the $Pd_{38}NC/Ni(OH)_2$-G (bond length: 4.92%) system (Table 2). These results imply that the first step of HCOOH dehydrogenation in $Pd_{38}NC$ proceeds to $HC\underline{O}O\underline{H}_a$*→$HC\underline{OO}_a$*+H* and the first step of that in the $Pd_{38}NC/Ni(OH)_2$-G system proceeds to $\underline{H}COO\underline{H}_b$*→$\underline{H}C\underline{O}O_b$*+H*. Next, in $Pd_{38}NC$, $HC\underline{OO}_a$*+H* proceeds to $\underline{H}C\underline{O}O_b$*+H*, but in the $Pd_{38}NC/Ni(OH)_2$-G system, it proceeds directly to CO_2*+2H* to produce H_2(g). The C-H bond length of $HC\underline{OO}_a$* on $Pd_{38}NC$ was decreased by 1.61%. As the final step, the C-H bond length of $\underline{H}C\underline{O}O_b$* was decreased by 3.34% in the $Pd_{38}NC/Ni(OH)_2$-G system and increased by 3.57% in $Pd_{38}NC$. In the final step, the C-H bond length of $\underline{H}C\underline{O}O_b$* in $Pd_{38}NC$ was activated more than in $Pd_{38}NC/Ni(OH)_2$-G system; it will not exceed the difference in activation energy for the shortened reaction step in the $Pd_{38}NC/Ni(OH)_2$-G system.

When considering the C-H bond length of HCOOH* to proceed to the COOH pathway, it increased by 1.29% in the $Pd_{38}NC/Ni(OH)_2$-G system and by 2.32% in $Pd_{38}NC$. However, the increase was smaller than that of the previously described O-H bond length, which implies that both systems are favorable to the HCOO pathway. In addition, this is further supported by the stable adsorption of HCOO* on both systems rather than that of COOH* (Table 1).

Furthermore, in addition to the bond length comparison for the activity prediction, the activity may be affected by another factor like bending degree of molecules that can modify the polarity of the molecules [44]. Although there was no clear evidence indicating a strong relationship between the bending degree of molecules and the activation of adsorbates for the formic acid dehydrogenation in the current study, it would be necessary to take into account both bond length and bond bending degree for the activity prediction.

4. Electronic Structure Analysis

The d-band center and density of states (DOS) calculations were performed to accurately demonstrate the effect of $Ni(OH)_2$-G on the adsorption behavior of the adsorbates. The d-band center position near the Fermi level indicates the relative adsorption strength

Table 3. The d-band center values of Pd atoms for different locations of the catalytic surface (see Fig. 5)

Locations	d-band centers[a]	
	$Pd_{38}NC/Ni(OH)_2$-G	$Pd_{38}NC$
1st layer	−2.03	−1.79
2nd layer	−1.84	−1.83
3rd layer	−1.66	−1.67
H_{ads} site	−1.76	−1.78
Interface	−1.92	−1.82
Surface	−1.84	−1.77

[a]The d-bands below the Fermi level were only considered in the center value calculation.

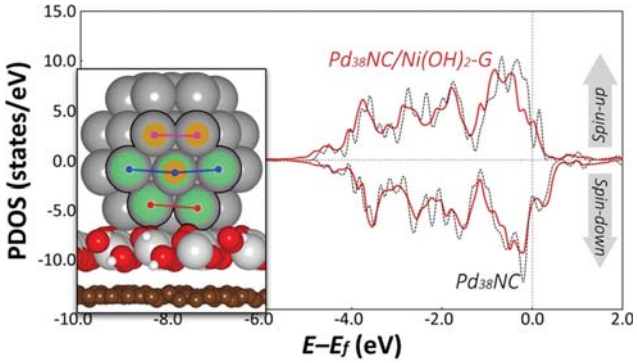

Fig. 5. Projected density of states (PDOS) of Pd d-bands of the $Pd_{38}NC/Ni(OH)_2$-G (red solid line) and $Pd_{38}NC$ (black dotted line) systems. The examined locations are marked in the $Pd_{38}NC/Ni(OH)_2$-G structure (left bottom side); Red, blue, and purple dotted lines represent the 1st, 2nd, and 3rd layers, respectively, and areas colored in orange, black, and green represent the H_{ads}, interface and surface sites (Table 3).

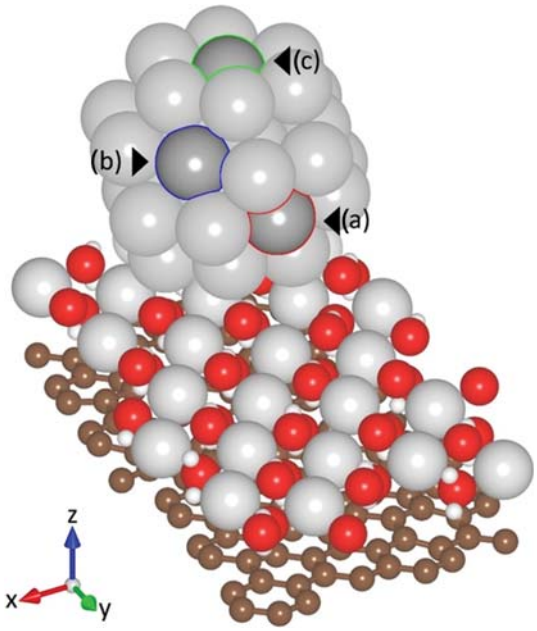

Fig. 6. Vacancy formation sites on the $Pd_{38}NC/Ni(OH)_2$-G system. (a), (b), and (c) indicate the vacancy sites where Pd atom was extracted.

of adsorbates on the transition metals. A more shifted d-band center toward the Fermi level represents a stronger reactivity [45,46].

We confirmed that the presence of $Ni(OH)_2$-G significantly influenced the activity of $Pd_{38}NC$. As shown in Table 3, the d-band center values of the $Pd_{38}NC/Ni(OH)_2$-G system show a wider range of values than that of $Pd_{38}NC$, which implies that the catalytic surface of $Pd_{38}NC/Ni(OH)_2$-G has various adsorption properties. It may be noted that at the interface site where the reaction mainly occurs, the d-band center of the $Pd_{38}NC/Ni(OH)_2$-G system is further (negatively) shifted from the Fermi level than that of $Pd_{38}NC$ (Table 3). This can explain the weaker adsorption strength of $HC\underline{OO}_a$* in the $Pd_{38}NC/Ni(OH)_2$-G system. Additionally, although the d-band center values at the H_{ads} sites of both systems are almost the same, a slight proximity of $Pd_{38}NC/Ni(OH)_2$-G towards the Fermi level may explain the stronger adsorption of H.

Note that many electrons were filled at a stable energy level below −5 eV in the $Pd_{38}NC/Ni(OH)_2$-G system compared to that in $Pd_{38}NC$ (Fig. 5). This implies that the electronic properties caused by $Ni(OH)_2$-G may have a positive effect on the surface stability, but may be a negative factor in providing a site for adsorbates to be adsorbed on a surface [47]. As a simple method to confirm this phenomenon, we compared the atomic distances of Pd atoms depending on the adsorption strength of adsorbates in each system (e.g., weakly and strongly adsorbed $HC\underline{OO}a$* on $Pd_{38}NC/Ni(OH)_2$-G and $Pd_{38}NC$, respectively). In the $Pd_{38}NC/Ni(OH)_2$-G system, the distance between Pd atoms was larger than that of $Pd_{38}NC$ when H was adsorbed on the surface. The distance between Pd atoms was smaller than that of $Pd_{38}NC$ when $HC\underline{OO}_a$* was adsorbed on the surface, which was identically confirmed in the case of $\underline{H}COO\underline{H}_b$*, which can shorten the reaction step. Detailed data are shown in the SI section 2. Thus, this implies that the electronic structure of $Pd_{38}NC$ modified by $Ni(OH)_2$-G can have a positive effect on the change in the distance between the Pd atoms on the surface. This weakened the adsorption strength of adsorbates that interact with a surface by their O atoms, requiring a relatively large size of adsorption site as well as strengthening that of H atoms requiring a small surface area. Thus, $Ni(OH)_2$-G can provide favorable properties for the adsorption of adsorbates, thereby improving the efficiency of HCOOH dehydrogenation and positively affecting the stability of the Pd surface.

5. Surface Stability of $Pd_{38}NC/Ni(OH)_2$-G

The enhanced stability of $Pd_{38}NC$ by $Ni(OH)_2$-G was also demonstrated by the results of Pd vacancy formation energy calculations. A Pd vacancy site in each system was selected at the site fairly similar to a flat surface (Fig. 6). The vacancy formation energy values of the $Pd_{38}NC/Ni(OH)_2$-G system were 0.76 (Fig. 6(a)), 0.46 (Fig. 6(b)), and 0.29 eV (Fig. 6(c)), respectively, at each site designed by three vacancy models based on the distance between $Pd_{38}NC$ and $Ni(OH)_2$-G. The $Pd_{38}NC$ system showed a negative vacancy formation energy of −0.73 eV (the vacancy site of the $Pd_{38}NC/Ni(OH)_2$-G system is the same position in $Pd_{38}NC$). The negative value of $Pd_{38}NC$ would only be interpreted as a relatively weaker formation energy compared to those examined, because the formation energy value can be sufficiently varied depending on the definition of Pd atom energy (e.g., it can be obtained from the bulk Pd structure or from a single Pd atom). It may be noted that the farther the Pd location from $Ni(OH)_2$-G, the lower the vacancy formation energy. This may imply that $Ni(OH)_2$-G can play an important role in enhancing the Pd surface stability.

CONCLUSION

We have designed and optimized a $Pd_{38}NC/Ni(OH)_2(100)$-graphene catalyst for the dehydrogenation of formic acid (HCOOH). The most stable adsorption configuration, $\underline{H}COO\underline{H}_b$*, was found on the $Pd_{38}NC/Ni(OH)_2$-G system, which was attributed to the modification of the electronic structure by $Ni(OH)_2$-G. The initial

adsorption behaviors of HCOOH* and its intermediate species, $HC\underline{O}O_a$* and $\underline{H}C\underline{O}O_b$*, which is the most important step for the entire HCOOH dehydrogenation reaction, was examined. It was confirmed that the HCOOH dehydrogenation on the $Pd_{38}NC/Ni(OH)_2(100)$-graphene would proceed through the direct HCOO pathway, improving the efficiency of HCOOH dehydrogenation by shortening the reaction step of the HCOO pathway. These findings were supported by the density of states and d-band center calculations, and the results also demonstrated the possibility that $Ni(OH)_2$-G can enhance the surface stability of $Pd_{38}NC$ according to the comparison of the vacancy formation energy. This study not only provides an insight for designing large-scale catalysts, but also is a milestone in solving the challenges of analyzing the reaction mechanisms of large catalysts.

ACKNOWLEDGEMENTS

The current work is supported by Technology Development Program to Solve Climate Changes of the National Research Foundation (NRF) funded by the Ministry of Science, ICT & Future Planning (2015M1A2A2074688).

NOTES

The authors declare no competing financial interests.

SUPPORTING INFORMATION

Additional information as noted in the text. This information is available via the Internet at http://www.springer.com/chemistry/journal/11814.

REFERENCES

1. J. Yang, A. Sudik, C. Wolverton and D. J. Siegel, *Chem. Soc. Rev.*, **39**, 656 (2010).
2. M. Grasemann and G. Laurenczy, *Energy Environ. Sci.*, **5**, 8171 (2012).
3. A. K. Singh, S. Singh and A. Kumar, *Catal. Sci. Technol.*, **6**, 12 (2016).
4. A. Boddien, B. Loges, F. Gärtner, C. Torborg, K. Fumino, H. Junge, R. Ludwig and M. Beller, *J. Am. Chem. Soc.*, **132**, 8924 (2010).
5. D. Mellmann, P. Sponholz, H. Junge and M. Beller, *Chem. Soc. Rev.*, **45**, 3954 (2016).
6. J. A. Herron, J. Scaranto, P. Ferrin, S. Li and M. Mavrikakis, *ACS Catal.*, **4**, 4434 (2014).
7. D. A. Bulushev, S. Beloshapkin and J. R. H. Ross, *Catal. Today*, **154**, 7 (2010).
8. M. Hattori, H. Einaga, T. Daio and M. Tsuji, *J. Mater. Chem. A*, **3**, 4453 (2015).
9. Y. Huang, X. Zhou, M. Yin, C. Liu and W. Xing, *Chem. Mater.*, **22**, 5122 (2010).
10. G. Chen, Y. Zhao, G. Fu, P. N. Duchesne, L. Gu, Y. Zheng, X. Weng, M. Chen, P. Zhang, C.-W. Pao, J.-F. Lee and N. Zheng, *Science*, **344**, 495 (2014).
11. R. Subbaraman, D. Tripkovic, D. Strmcnik, K.-C. Chang, M. Uchimura, A. P. Paulikas, V. Stamenkovic and N. M. Markovic, *Science*, **334**, 1256 (2011).
12. R. Subbaraman, D. Tripkovic, K.-C. Chang, D. Strmcnik, A. P. Paulikas, P. Hirunsit, M. Chan, J. Greeley, V. Stamenkovic and N. M. Markovic, *Nat. Mater.*, **11**, 550 (2012).
13. W. Huang, H. Wang, J. Zhou, J. Wang, P. N. Duchesne, D. Muir, P. Zhang, N. Han, F. Zhao, M. Zeng, J. Zhong, C. Jin, Y. Li, S.-T. Lee and H. Dai, *Nat. Commun.*, **6**, 10035 (2015).
14. J.-M. Yan, Z.-L. Wang, L. Gu, S.-J. Li, H.-L. Wang, W.-T. Zheng and Q. Jiang, *Adv. Energy Mater.*, **5**, 1500107 (2015).
15. Q. Sun, N. Wang, Q. Bing, R. Si, J. Liu, R. Bai, P. Zhang, M. Jia and J. Yu, *Chem.*, **3**, 477 (2017).
16. R. Kou, Y. Shao, D. Mei, Z. Nie, D. Wang, C. Wang, V. V. Viswanathan, S. Park, I. A. Aksay, Y. Lin, Y. Wang and J. Liu, *J. Am. Chem. Soc.*, **133**, 2541 (2011).
17. R. I. Jafri, N. Rajalakshmi and S. Ramaprabhu, *J. Mater. Chem.*, **20**, 7114 (2010).
18. L. Dong, R. R. S. Gari, Z. Li, M. M. Craig and S. Hou, *Carbon*, **48**, 781 (2010).
19. M. J. Allen, V. C. Tung and R. B. Kaner, *Chem. Rev.*, **110**, 132 (2010).
20. K. S. Novoselov, A. K. Geim, S. V. Morozov, D. Jiang, Y. Zhang, S. V. Dubonos, I. V. Grigorieva and A. A. Firsov, *Science*, **306**, 666 (2004).
21. D.-H. Lim, A. S. Negreira and J. Wilcox, *J. Phys. Chem. C*, **115**, 8961 (2011).
22. D.-H. Lim and J. Wilcox, *J. Phys. Chem. C*, **115**, 22742 (2011).
23. D.-H. Lim, J. H. Jo, D. Y. Shin, J. Wilcox, H. C. Ham and S. W. Nam, *Nanoscale*, **6**, 5087 (2014).
24. D. Y. Shin, M.-S. Kim, J. A. Kwon, Y.-J. Shin, C. W. Yoon and D.-H. Lim, *J. Phys. Chem. C*, **123**, 1539 (2019).
25. H. Wang, H. S. Casalongue, Y. Liang and H. Dai, *J. Am. Chem. Soc.*, **132**, 7472 (2010).
26. G. Kresse and J. Furthmüller, *Phys. Rev. B*, **54**, 11169 (1996).
27. G. Kresse and D. Joubert, *Phys. Rev. B*, **59**, 1758 (1999).
28. P. E. Blöchl, *Phys. Rev. B*, **50**, 17953 (1994).
29. J. P. Perdew, K. Burke and M. Ernzerhof, *Phys. Rev. Lett.*, **77**, 3865 (1996).
30. H. J. Monkhorst and J. D. Pack, *Phys. Rev. B*, **13**, 5188 (1976).
31. M. Methfessel and A. T. Paxton, *Phys. Rev. B*, **40**, 3616 (1989).
32. A. J. Tkalych, K. Yu and E. A. Carter, *J. Phys. Chem. C*, **119**, 24315 (2015).
33. S. Grimme, *J. Comput. Chem.*, **27**, 1787 (2006).
34. M. Sakurai, K. Watanabe, K. Sumiyama and K. Suzuki, *J. Chem. Phys.*, **111**, 235 (1999).
35. K. G. Dyall, *Theoretical Chemistry Accounts*, **117**, 459 (2007).
36. J. G. Howalt, T. Bligaard, J. Rossmeisl and T. Vegge, *Phys. Chem. Chem. Phys.*, **15**, 7785 (2013).
37. V. Y. Kazimirov, M. B. Smirnov, L. Bourgeois, L. Guerlou-Demourgues, L. Servant, A. M. Balagurov, I. Natkaniec, N. R. Khasanova and E. V. Antipov, *Solid State Ionics*, **181**, 1764 (2010).
38. G. Mukhopadhyay and H. Behera, *arXiv:1306.0809* (2013).
39. J. Yan, Q. Wang, T. Wei and Z. Fan, *Adv. Energy Mater.*, **4**, 1300816 (2014).
40. Z. Wu, X.-L. Huang, Z.-L. Wang, J.-J. Xu, H.-G. Wang and X.-B. Zhang, *Sci. Rep.*, **4**, 3669 (2014).
41. Y. Qi, Y. Liu, R. Zhu, Q. Wang, Y. Luo, C. Zhu and Y. Lyu, *New J. Chem.*, **43**, 3091 (2019).

42. J. S. Yoo, F. Abild-Pedersen, J. K. Nørskov and F. Studt, *ACS Catal.*, **4**, 1226 (2014).
43. P. Wang, S. N. Steinmann, G. Fu, C. Michel and P. Sautet, *ACS Catal.*, **7**, 1955 (2017).
44. H. Xu, W. Chu, W. Sun, C. Jiang and Z. Liu, *RSC Adv.*, **6**, 96545 (2016).
45. B. Hammer and J. K. Nørskov, *Surf. Sci.*, **343**, 211 (1995).
46. B. Hammer and J. K. Nørskov, *Adv. Catal.*, **45**, 71 (2000).
47. A. Vojvodic, J. Nørskov and F. Abild-Pedersen, *Top. Catal.*, **57**, 25 (2014).

Supporting Information

Hybrid Pd_{38} nanocluster/$Ni(OH)_2$-graphene catalyst for enhanced HCOOH dehydrogenation: First principles approach

Dong Yun Shin*, Min-Su Kim*, Sukho Kang*, Jeong An Kwon*, Thillai Govindaraja*, Chang Won Yoon,***,†, and Dong-Hee Lim*,†**

*Department of Environmental Engineering, Chungbuk National University, Cheongju 28644, Korea
**Center for Hydrogen and Fuel Cell Research, Korea Institute of Science and Technology, Seoul 02792, Korea
***KHU-KIST Department of Converging Science and Technology, Kyung Hee University, Seoul 02447, Korea
(*Received 30 March 2020 • Revised 23 May 2020 • Accepted 4 June 2020*)

1. Candidates of $Ni(OH)_2$-G Systems

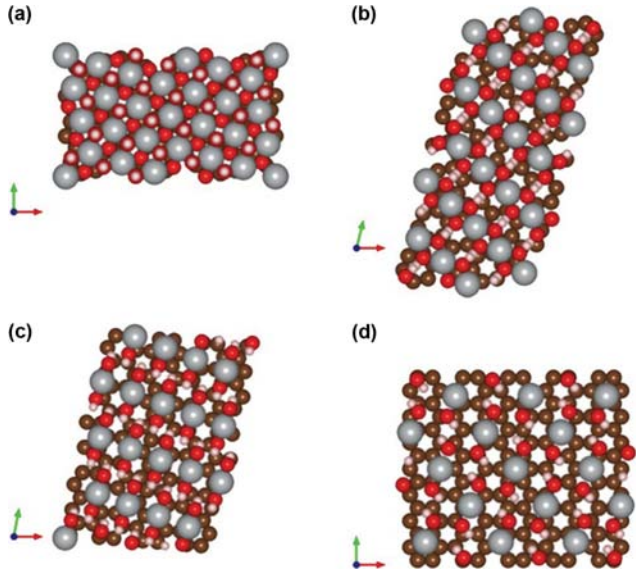

Fig. S1. Top views of the designed (a) $Ni(OH)_2$(001)-G, (b) $Ni(OH)_2$ (100)-G, (c) $Ni(OH)_2$(101)-G, and (d) $Ni(OH)_2$(110)-G. Grey, brown, red, and white spheres represent Ni, C, O, and H, respectively.

2. Interatomic Distances of Pd Atoms the Pd_{38}NC with and without $Ni(OH)_2$-G

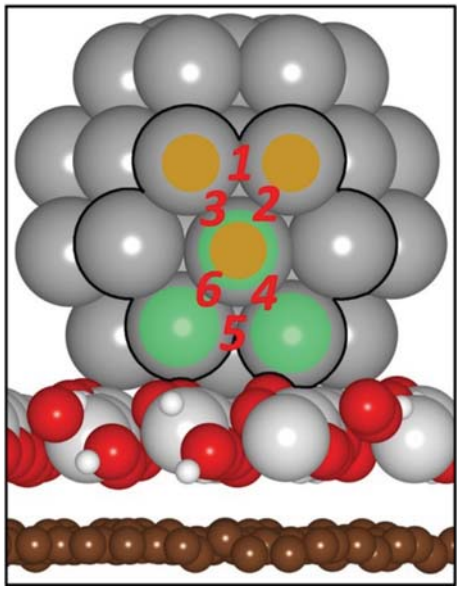

Fig. S2. Adsorption sites of adsorbates on the Pd_{38}NC/$Ni(OH)_2$-G system. Sites colored in orange and green represent H and other adsorbates, respectively.

Table S1. Interatomic distances of Pd atoms on Pd_{38}NC/$Ni(OH)_2$-G and Pd_{38}NC systems. The numbers indicate the site shown in Fig. S2

Adsorbate	Pd_{38}NC/$Ni(OH)_2$-G			Pd_{38}NC		
	1	2	3	4	5	6
H*	2.6082	2.7223	2.7732	2.6063	2.7157	2.7647
HC$\underline{O}O_a$*	2.7333	2.8290	2.5539	2.8553	2.7935	2.8458
HC$\underline{O}O\underline{H}_a$*	2.7292	2.8360	2.5647	2.7246	2.7984	2.6251
$\underline{H}COO\underline{H}_b$*	2.8269	2.8253	2.6751	2.8213	2.8065	2.6846